Fabrication of sub-micron pillars on curved surfaces using thermal nanoimprint lithography

Thesis report

Dionysios Rompolas

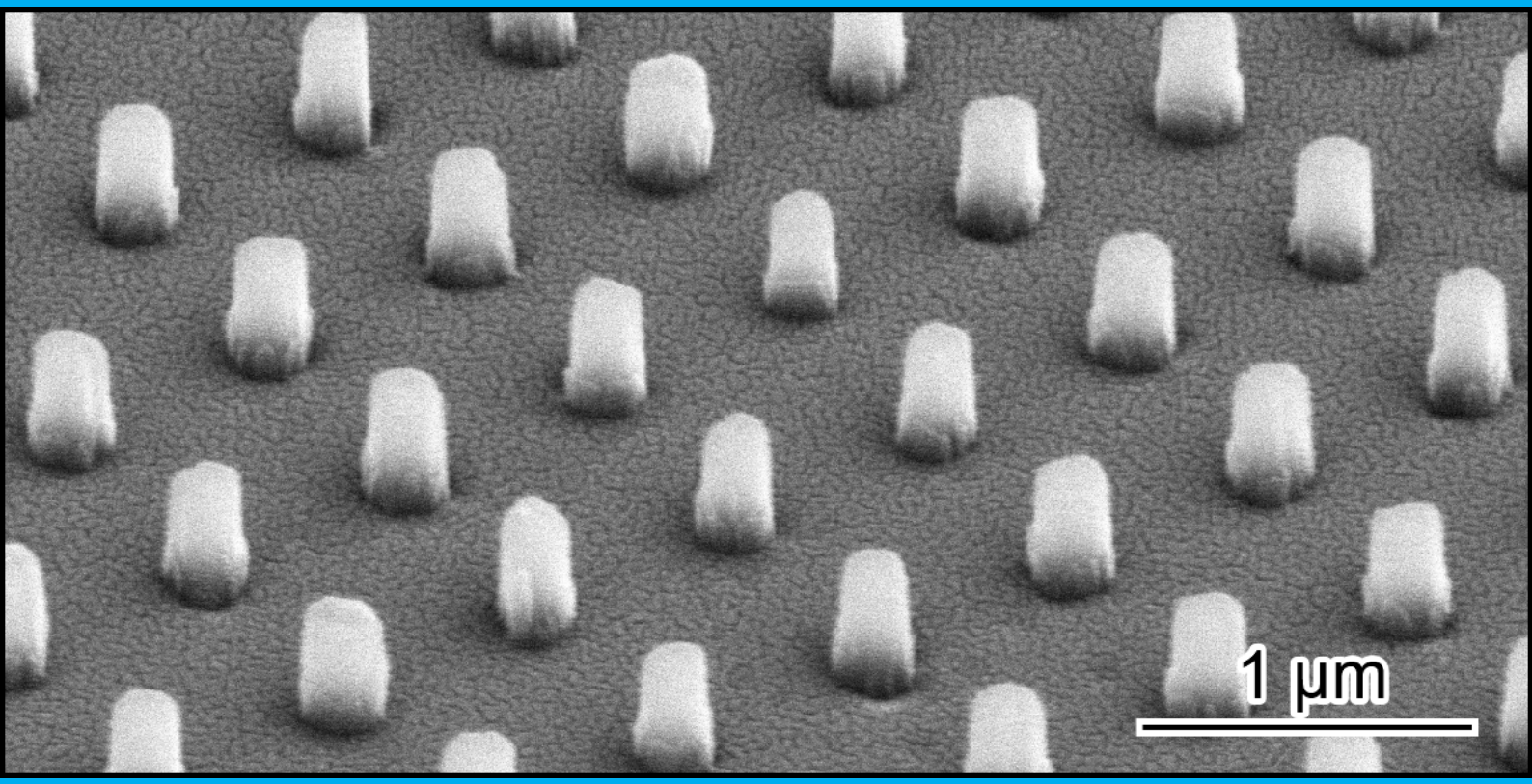

TU Delft

Fabrication of sub-micron pillars on curved surfaces using thermal nanoimprint lithography

Thesis report

by

Dionysios Rompolas

Student number: 5141958

to obtain the degree of Master of Science
at the Delft University of Technology,
to be defended publicly on Thursday August 4, 2021 at 9:00 AM.

Thesis supervisors:	Dr. ir. Lidy E. Fratila-Apachitei,	TU Delft
	Prof. Dr. ir. Amir A. Zadpoor,	TU Delft
	PhD candidate Mahya Ganjian,	TU Delft

TU Delft

Acknowledgements

The work presented here was conducted under the supervision of Dr. ir. Lidy E. Fratila-Apachitei, Prof. Dr. ir. Amir A. Zadpoor, and PhD candidate Mahya Ganjian. I thank all of them for the opportunity they gave me to work in such an interesting field of science and for the help, guidance, and training along the way. Also, I want to thank Dr. Cornelis W. Hagen (Kees) for the access to the SEM equipment, Dustin Laur for the training and assistance with the SEM equipment, and Rob Luttjeboer for the assistance in the chemical lab. Finally, I thank every other person who contributed to this work and the TU Delft for the facilities and resources that were necessary to complete this project.

Dionysios Rompolas
Delft, August 2021

Abstract

Studies have shown that pillars of specific dimensions and spatial arrangement can promote osteogenic differentiation of stem cells and kill bacteria that cause infections. Other studies have shown that surface curvature can also serve as a mechanical cue to modulate cell behavior. Therefore, the fabrication of pillars on curved surfaces would allow researchers to investigate the synergistic effect of pillars and curvature on cell behavior.

In this project, a process was developed based on thermal nanoimprint lithography (TNL) and dry etching techniques for the fabrication of pillars into curved substrates made of hard materials. To this aim, a fused silica specimen containing sub-micron pillars was used as the master mold in a molding process to replicate the pillars as pits into a hybrid polydimethylsiloxane (PDMS) mold. The dimensions and morphology of the replicated patterns were assessed using a scanning electron microscope (SEM). Thereafter, TNL was employed to imprint the pits of the hybrid PDMS mold on the surface of the desired planar/curved substrates. Finally, etching processes were employed to transfer the patterns into the bulk of the substrates. The process was first developed on planar fused silica substrates and then, on curved substrates.

The interspace of the resultant pillars on the planar substrates was no more than 3% different than the interspace of the original pillars on the master mold. The diameter was also close to the values of the diameter of the original pillars (the maximum difference was 23%). The height of the pillars differed slightly (mo more than 16%) for the specific process conditions that were used. On the curved substrates, the interspace increased by 5% and 10%, and the diameter by 57% and 11%.

Contents

1 Introduction

1.1. Patterns with interesting functions

Surfaces with micro-and nanoscale patterns are widely existent in nature [1–5]. Such surfaces possess properties that would be desirable in a wide range of applications and devices. Butterflies of the Morpho species, which are known for the beautiful colors of their wings, possess ordered arrays of nanostructures on their wings' surface that show different optical responses to different vapors and vapor concentrations [1]. Their response outperforms current nanofabricated sensors and could be mimicked for the design of new optical gas sensors [1]. Moth eyes consist of an array of parabolic hemispheres in the nanoscale and are characterized by their antireflection properties [2]. Such surfaces are ideal in energy-related applications that require minimum light reflection like solar thermal and photovoltaic systems [3]. The lotus effect, also known as the self-cleaning effect of the lotus leaf, is a phenomenon attributed to micro-and nanoscale structures on the surface of the lotus leaves [4]. These structures create a highly hydrophobic surface which when wetted causes water drops to bead up and flow away, carrying away dirt from the leaves [4]. This effect can be applied in the fields of self-cleaning windows, solar panels, buildings, and windshields [5].

Apart from the natural existing micro-and nanopatterns and their potential employment in different fields, other kinds of patterns have been demonstrated to give surfaces unique properties and/or cause desired interactions with materials. In the field of optics, patterns can improve antireflection and increase the mechanical endurance of the optical surface [6] with application in optical components, photovoltaic systems, and light-emitting diodes [7]. In biological research, patterns have been shown to control cell behavior (migration, differentiation, proliferation, death) [8–10] and can be integrated into medical implants [11] or used for regenerative medicine studies [12].

Patterning techniques have been well established for patterning planar surfaces. Soft lithography, photolithography, electron beam lithography (EBL), and direct laser writing - separately or in combination - are some techniques that have been developed to create, replicate, and transfer high-resolution patterns. Recently, there is an emerging trend in patterning non-planar surfaces. This is due to the fact that in many applications there are non-planar components, sometimes with complicated geometries. In optics, for applications such as tomography or microscopy, some of the device components are curved lenses [13]. In the sector of photovoltaic systems, new technologies emerge that use curved panels

for energy harvesting [14]. In orthopedics, bone implant (e.g., hip replacement prosthesis) surfaces are curved. In electronics, flexible sensors and circuits that conform with non-planar surfaces are fabricated [15]. So, the need to adapt current techniques or develop new ones for patterning non-planar surfaces is evident.

1.2. Patterning curved surfaces using thermal nanoimprint lithography (TNL)

Patterning techniques have been well established over the years for planar surfaces and recently, some of them have been employed on curved surfaces as well. Among the plethora of techniques, soft lithographic ones are dominant when it comes to patterning of non-planar surfaces. Soft lithography is a family of techniques that create (replicate) structures using soft flexible molds. The molds are made of elastomeric materials, most notably PDMS and thus, they make it possible to pattern non-planar surfaces that cannot be performed with traditional rigid planar molds. These techniques are capable of constructing features ranging from hundreds of micrometers to tens of nanometers [16].

A well-known and widely used soft lithographic technique is TNL. TNL is a hot embossing process (Figure 1.1) where the mold is a flexible patterned stamp when patterning curved surfaces, most often made of PDMS [17]. In TNL, the flexible mold is brought in conformable contact and under high pressure with the substrate which is a solid rigid surface [17]. At the same time, the substrate is heated to above its glass transition temperature (T_g) until the material which the substrate is made of (or coated with) softens, deforms, and fills the stamps' micro-and nanostructures [17]. After a specific amount of time and when the patterns have been imprinted into the substrate, the temperature drops gradually and the stamp is peeled off [17].

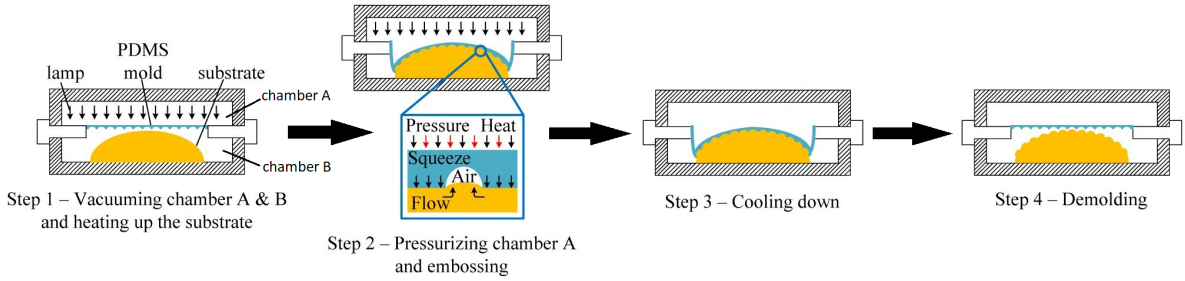

Figure 1.1. Schematic illustration of TNL [17].

Using this method, Chen *et. al.* [17] fabricated a microlens array (Figure 1.2 a) on the surface of a convex polymethylmethacrylate (PMMA) substrate and gratings on the surface of a concave PMMA substrate using a PDMS mold. The microlenses had a diameter of 187 µm and a height of 13.29 µm [17]. Choi *et. al.* [18] managed to create features (pits and gratings) on a cylinder with a diameter of 8 mm and on a spherical surface with a diameter of 20 mm (Figure 1.2 b). The diameter of the pits was 400 nm and the width of the gratings was 350 nm [18]. The two substrates were made of glass, their surfaces were coated with polystyrene (PS), and the mold was made of PDMS [18]. The imprinting was performed by heating the substrate above its T_g and placing the PDMS mold on top of the PS layer by applying pressure with the fingers [18]. Bhingardive *et. al.* [19] patterned a spherical glass lens

(radius of curvature (ROC) of 50 mm) (dip-coated with poly benzyl methacrylate(PBMA)) with nanopits of an average diameter of 100 nm (Figure 1.2 c).

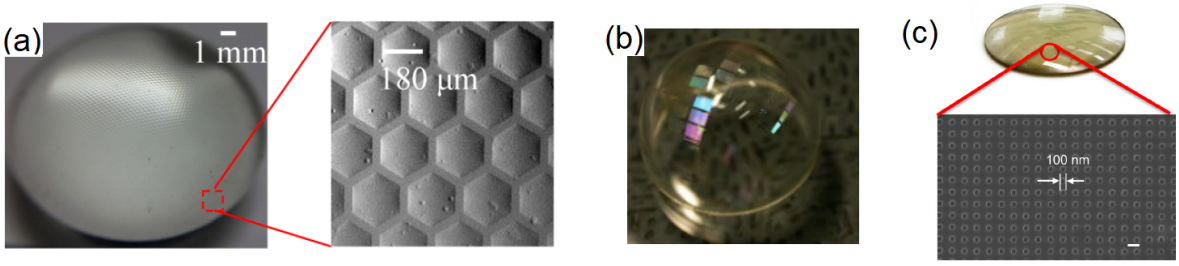

Figure 1.2. Micro-and nanopatterns on curved surfaces fabricated by TNL. (a) Microlenses on the surface of a PMMA lens [17]. (b) PS patterns on a glass spherical surface of 20 mm diameter [18]. (c) PBMA nanopits on a glass lens with an ROC of 50 mm [19].

1.3. Purpose of the project

TNL is an appealing technique for the fabrication of patterns on non-planar surfaces. It combines the benefits of soft lithography (*i.e.*, patterning of non-planar surfaces, high-resolution patterning, low cost, simple or no equipment required, and the possibility to use the mold multiple times) with control over the dimensions of the patterns, parameters such as temperature and imprinting force, and following etching steps. To our knowledge and after examining the literature, we found out that researchers who create patterns on non-planar surfaces with this technique use the patterns directly after thermal nanoimprinting [17–19]. In other words, the patterns are made of the imprinting material (*e.g.*, PMMA, PBMA, PS). They do not proceed to additional micro-and nanofabrication processes such as deposition, etching, and lift-off in order to transfer the patterns into the substrate underneath.

In the field of bone-implants, recent studies have shown that pillars can modulate the behavior of cells related to or affecting bone healing [8]. More specifically, ordered pillars of standard dimensions can promote osteogenic differentiation of stem cells accelerating the healing process and at the same time damage and kill bacteria that are associated with infections [8]. Therefore, the integration of pillars on the curved surfaces of bone implants is of interest. Additionally, microscale curvature has also been proven to affect cell behavior as reported by Callens *et al.* [20]. Therefore, incorporating curvature and pillars into one structure holds great research value.

So far, sub-micron and nanopillars have been fabricated on planar surfaces and their properties have been evaluated [21]. This report presents the work that was conducted in an attempt to develop and establish a process based on TNL and etching techniques for the fabrication of curved substrates containing pillars made of hard materials (*i.e.*, fused silica).

2

Materials and Methods

2.1. Master mold

Planar fused silica specimens containing two arrays of sub-micron pillars with center-to-center interspaces of 700 nm and 1 µm (master mold) (Figure 2.1) were fabricated by EBL. The process steps involved in fabricating pillars on the specimens were not part of the present work, therefore, no more detail will be given here. The dimensions of the master mold were 1x1 cm^2, with a thickness of 500 µm, and the size of each array of pillars was 3x5 mm^2.

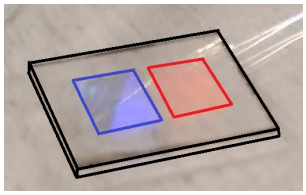

Figure 2.1. Planar fused silica master mold containing two arrays of pillars. In the image, the master mold and the arrays are outlined. The arrays, like the rest of the master mold, are transparent. The colors they have in the image are the result of the interaction between the pillars and light.

Tilted and top view SEM images of the two arrays of pillars on the fused silica master mold with the designed interspaces of 700 nm and 1 µm are illustrated in Figure 2.2. The height and diameter of the pillars were measured using tilted view SEM images and the interspace of the two arrays was measured using top view SEM images. The results are presented in Table 2.1.

	700 nm	1 µm
interspace (nm)	717 ± 22	1026 ± 17
height (nm)	671 ± 31	702 ± 64
diameter (nm)	311 ± 9	317 ± 14
aspect ratio (AR)	2.15 ± 0.10	2.21 ± 0.18

Table 2.1. Dimensions of the pillars of the master mold.

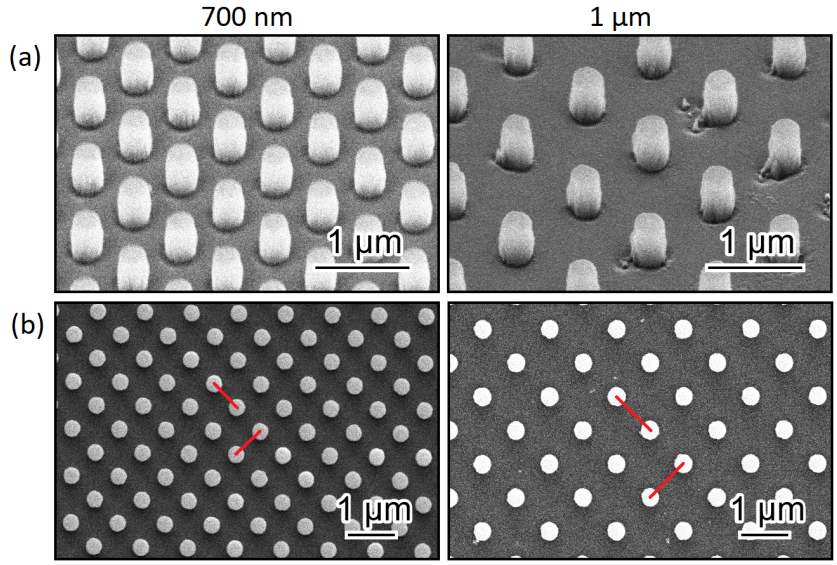

Figure 2.2. (a) 45° tilted view and (b) top view SEM images of the pillars of the master mold. The red lines indicate the interspace.

2.2. Fabrication of hybrid PDMS mold by replica molding

The master mold was used in a replica molding process to fabricate a hybrid PDMS mold containing pits (Figure 2.3) (Appendix A). Initially, hard PDMS (hPDMS) was poured into the master mold, spin-coated at 1000 rpm for 40 sec, and baked at 60 °C for 20 min to create a negative replica of the pillars (Figure 2.3 b). Next, PDMS was poured on top of the hPDMS layer and baked at 40 °C for 16 hrs to create a composite hPDMS/PDMS layer (Figure 2.3 c). Finally, the resultant hybrid PDMS mold containing pits was gently peeled off from the master mold (Figure 2.3 d).

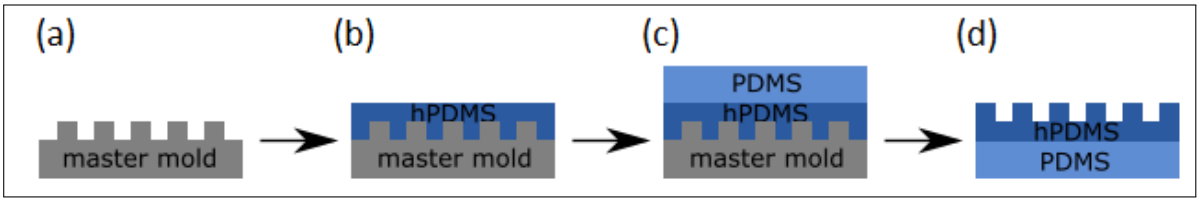

Figure 2.3. Schematic illustration of replica molding. a) Master mold containing pillars serving as mold. b) Pouring hPDMS into the mold. c) Pouring PDMS on top of the hPDMS layer. d) Demolding of hybrid PDMS mold containing pits.

2.3. Pattern transfer into the final substrate using TNL

2.3.1. Fabrication process to transfer patterns into a planar substrate

The process developed for the fabrication of pillars on a planar fused silica substrate incorporated material deposition, imprinting, and material etching techniques (Figure 2.4).

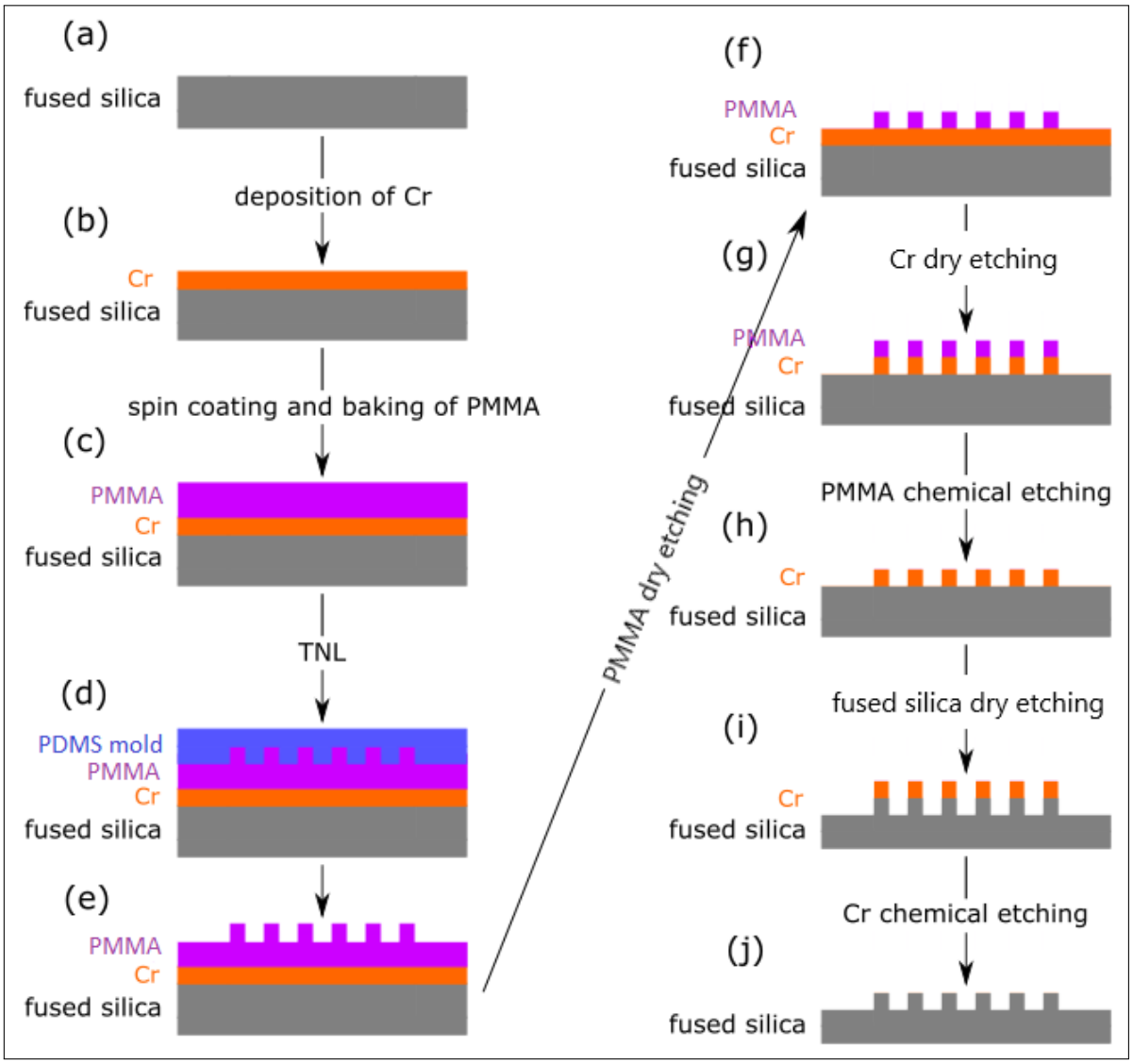

Figure 2.4. Schematic illustration of the fabrication process developed to transfer patterns into a planar substrate.

2.3.1.1. Substrate preparation

Initially, a planar fused silica substrate was cleaned in an ultrasonic bath, first in acetone for 30 min, then in isopropyl alcohol (IPA) for 30 min, and finally, in deionized (DI) water for 30 min. Subsequently, it was dried using compressed N_2 gas. Next, a thin layer of Cr (30 nm) was deposited on the substrate using electron beam physical vapor deposition (EBPVD) (Temescal FC-200, Ferrottec, USA) at a rate of 0.1 nm/sec and a pressure of $1.5{\cdot}10^{-6}$ Torr (Figure 2.4 b). Then, PMMA (950A3, MicroChem Corp., USA) was spin-coated on the substrate at 3500 rpm and baked at 185 °C for 20 min (Figure 2.4 c). The thickness of the resultant PMMA layer was measured using a profilometer (Dektak, Bruker, USA). To do so, a scratch was made on the substrate with a pair of tweezers and then, the depth of the scratch was measured by the profilometer. The thickness of the PMMA layer was defined as the depth of the scratch, which was about 130 nm.

2.3.1.2. Thermal nanoimprint lithography

TNL is the primary patterning technique of the process that creates the initial patterns on the substrate (Figure 2.4 d, e). The system used for the imprinting (EVG520, EV Group, Austria) consisted of two plates (top and bottom) (Figure 2.5 a). The substrate was placed between the plates and the imprinting force was applied to it in a "sandwich" like manner (Figure 2.5 b).

Thermal imprinting begins from ambient temperature ($T_{ambient}$ in Figure 2.5 c) and rises to the imprinting temperature (*i.e.*, 140 °C and 180 °C) (T_{imp} in Figure 2.5 c) at a rate of 2 °C/min. When T_{imp} is reached, a force of 250 N is applied (Figure 2.5 c). The temperature is kept at T_{imp} for 165 sec and then, the system is cooled down (Figure 2.5 c). At 80 °C (demolding temperature), the force is released (Figure 2.5 c). When the temperature reaches 40 °C, the sample is removed from the system and the hybrid PDMS mold is peeled off.

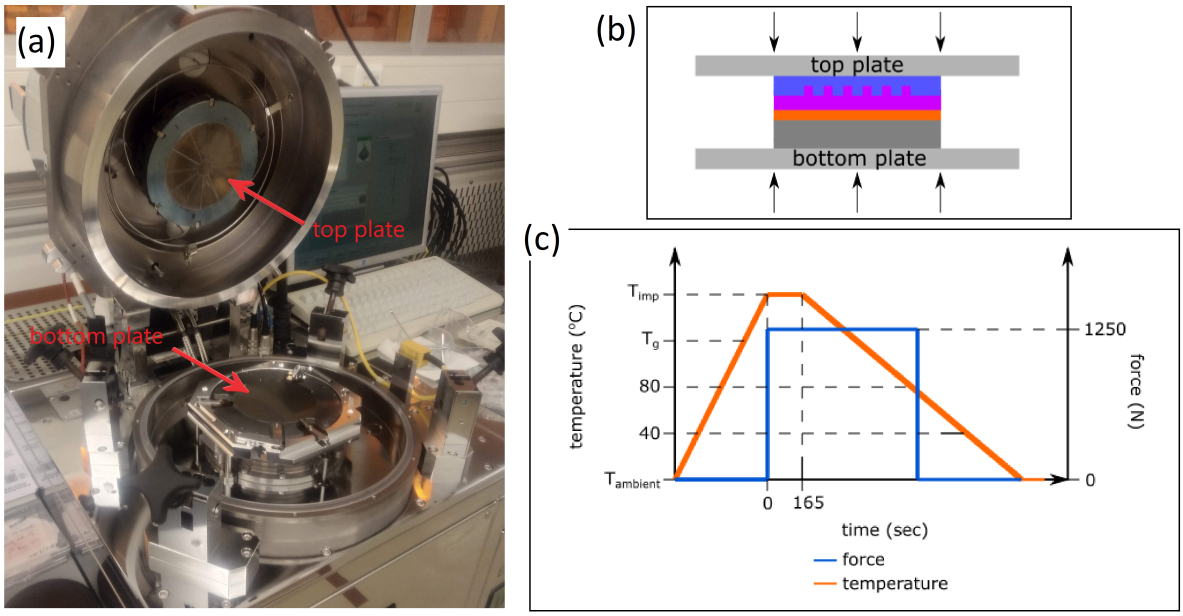

Figure 2.5. a) Image of the thermal imprinting system. b) Schematic illustration of the imprinting setup. c) Thermal imprinting process curve.

2.3.1.3. Reactive ion etching

Reactive ion etching (RIE) is a technique used to selectively etch materials. The mask protects parts of the sample where no etching is desirable and exposes the rest. In RIE the sample is exposed to a gas mixture where the gases are selected according to the material to be etched. Then, two electrodes create a radio frequency (RF) electromagnetic field that excites the gas mixture and generates plasma containing reactive species (ions and radicals) (Figure 2.6) [22]. At the same time, a voltage is created (between the plasma and the sample-carrying electrode) that accelerates and directs the ions towards the sample (Figure 2.6) [22]. Etching of material happens in two ways. The first way is chemically when ions and radicals react with the material creating volatile particles that are subsequently exhausted and the second way is physically when accelerated ions bombard the material and sputter out of it particles that are subsequently exhausted as well [22].

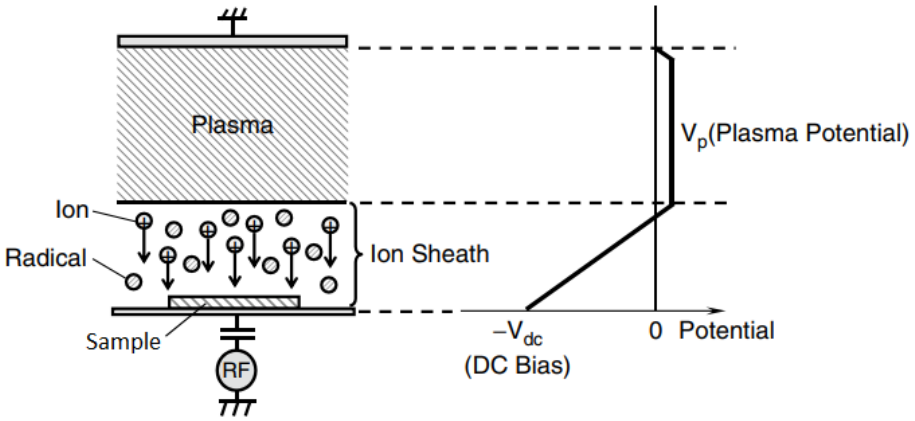

Figure 2.6. Schematic illustration of RIE [22].

After thermal nanoimprinting, the residual PMMA on the substrate was etched to reach the Cr layer (Figure 2.4 e, f) using O_2 plasma (Sentech Etchlab 200, SENTECH Instruments GmbH, Germany) (Table 2.2). The remaining PMMA pillars were used as a mask to etch Cr (Figure 2.4 f, g) using chlorine-based plasma RIE (Plasmalab System 100, Oxford Instruments, UK) on a 4 inch SiO_2 carrier wafer (Table 2.2). After dissolving the remaining PMMA mask in N-Methyl-2-pyrrolidone (NMP) (Sigma Aldrich, USA) at 80 °C overnight (Figure 2.4 g, h), the remaining Cr pillars were used as a mask to etch the fused silica substrate using fluorine-based inductively coupled plasma (ICP) RIE (Figure 2.4 h, i) (Adixen AMS 100 I-16 speeder, Alcatel, France) on a 4 inch Si carrier wafer (Table 2.2). Thus, pillars were successfully transferred into the final desired substrate (Figure 2.4 i). Finally, the Cr mask was chemically etched using Cr etchant (Chromium Etchant N1, MicroChemicals, Ulm, Germany) (Figure 2.4 j).

	PMMA RIE	Cr RIE	fused silica ICP RIE
O_2 flow (sccm)	20	5	-
Cl_2 flow (sccm)	-	50	-
C_4F_8 flow (sccm)	-	-	15
CH_4 flow (sccm)	-	-	15
He (sccm)	-	-	150
RF power 1 (W)	20	50	2500
RF power 2 (W)	-	-	250
temperature (°C)	-	40	0
pressure	0.04 mbar	12.5 µbar	0.01 mbar
time (min:sec)	2:00	1:30	3:30

Table 2.2. Process conditions of RIE steps.

2.3.2. Fabrication process to transfer patterns into a curved substrate

To transfer the pillars into the curved substrate, the previously described process was modified appropriately. Commercial plano-convex and concave lenses (110-0104E & 112-0105E, EKSMA OPTICS, Lithuania) made of BK7 glass served as curved substrates (Figure 2.7). The ROC of the convex lens was 10.4 mm and that of the concave lens was 13 mm.

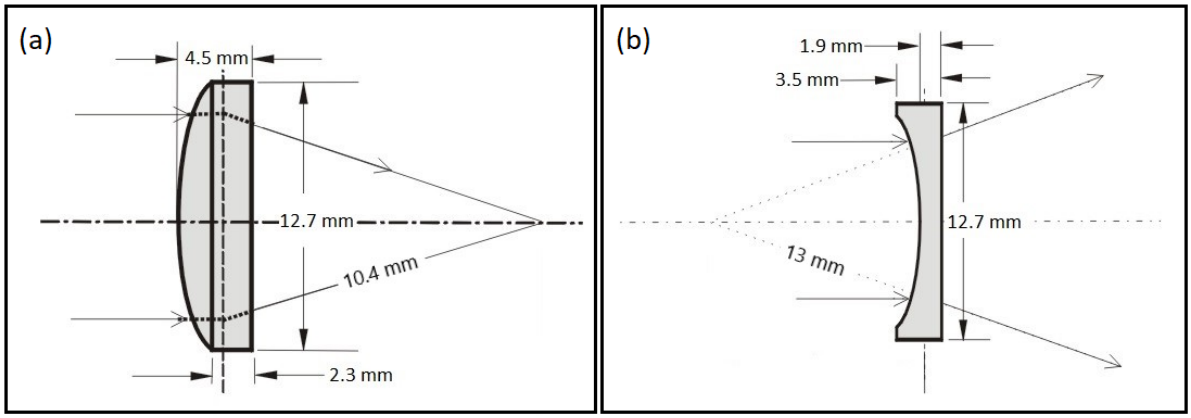

Figure 2.7. Drawings of the a) convex and b) concave lenses used in this study [23].

The same as the previous section, the substrates - lenses in this case - were cleaned in an ultrasonic bath in acetone, IPA, and DI water for 30 min in each solution. Subsequently, they were dried using compressed N_2 gas. For the fabrication of pillars on the curved substrates, the same process developed for the planar substrates was applied (Figure 2.9).

2.3.2.1. Thermal nanoimprint lithography

TNL on the curved substrates required specific setup adjustments. The first setup adjustment was adding an elastic PDMS support structure on top of the hybrid PDMS mold (support in Figure 2.8) (Appendix B). The second setup adjustment was the fabrication and use of peripheral elastic PDMS support structures which were added to the system along with the sample (peripheral support in Figure 2.8) (Appendix B). The process parameters were: imprinting force = 1250 N and 2500 N and imprinting temperature = 140 °C, 160 °C, and 180 °C. The rest of the process parameters were the same as the described values for the planar substrate.

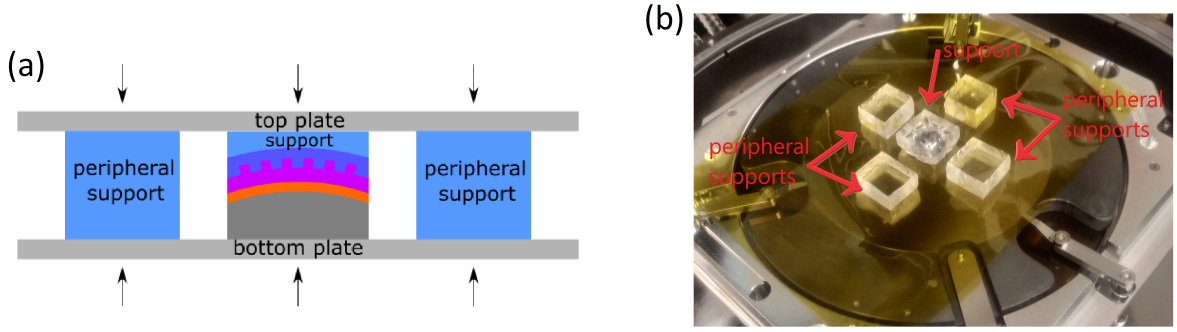

Figure 2.8. a) Schematic illustration of the imprinting setup for the curved substrate. b) Image of the imprinting setup on the curved substrate.

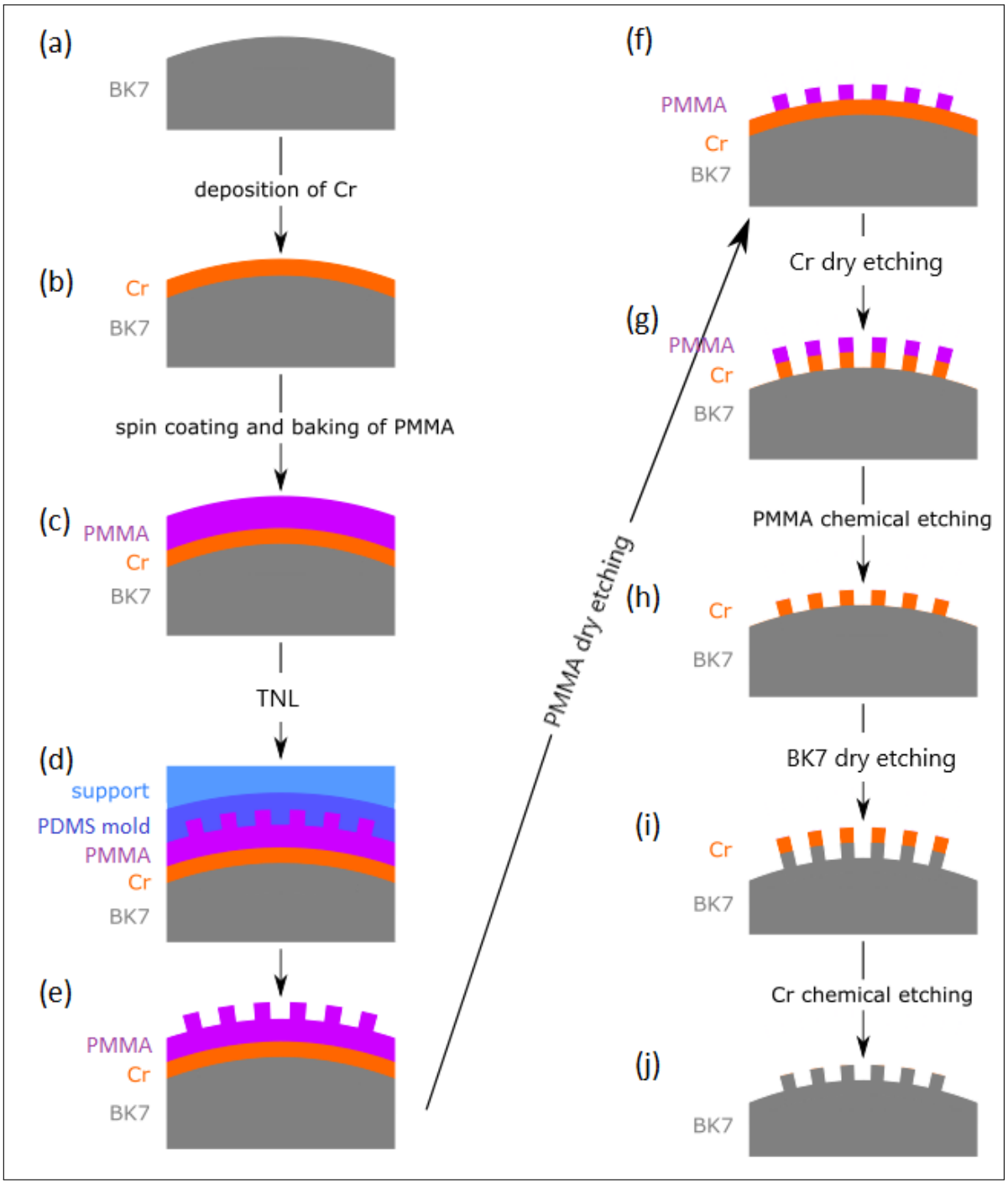

Figure 2.9. Schematic illustration of the fabrication process developed to transfer patterns into curved substrates.

2.4. Imaging and Characterization

Inspection of the samples was performed with a SEM (Helios G4 CX dual beam workstation, Hillsborough, FEI, USA). Specimens need to be electrically conductive to be imaged by SEM and therefore, before imaging, a thin layer of gold (13 nm thick) was sputtered on the specimens. SEM images were analyzed using Gwyddion (version 2.57) software and all

relevant parameters were measured (*i.e.*, pillar height and base diameter from 45° tilted view SEM images, and interspace from top view SEM images) and processed (Excel 2016, Microsoft Corp., USA).

3

Results

3.1. Fabrication of hybrid PDMS mold by replica molding

The resultant hybrid PDMS mold (Figure 3.1) was a negative replica of the master mold and contained pits orthogonally arranged in two arrays (Figure 3.2). The pits had a circular shape and the surface of the mold had a smooth morphology (Figure 3.2).

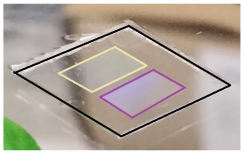

Figure 3.1. Hybrid PDMS mold containing pits as a result of replica molding of the master mold. In the image, the mold and the arrays are outlined.

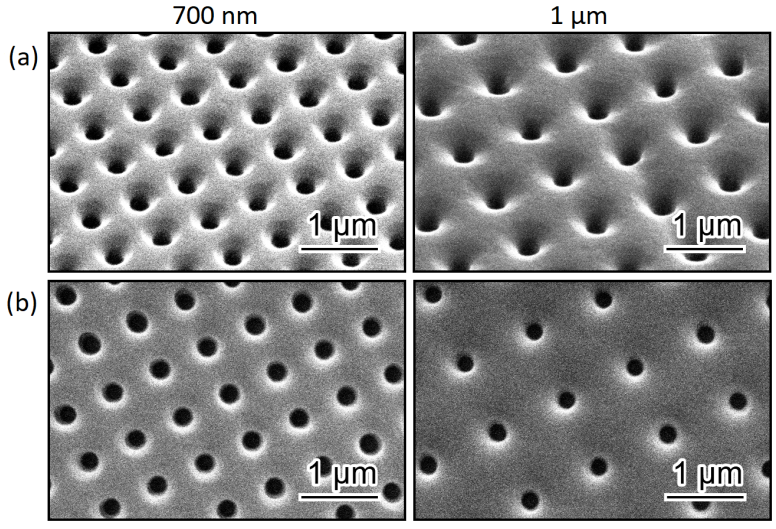

Figure 3.2. a) 45^{o} tilted view and b) top view SEM images of the hybrid PDMS mold containing pits.

The diameter of the pits was measured using tilted view SEM images and the interspacing between the pits was measured using top view SEM images. The depth was not measured since the bottom of the pits was not visible. A comparison between the size of

the resultant pits on the hybrid PDMS mold and the pillars on the master mold is shown in Figure 3.3. The diameter of the pits of the PDMS mold was 21% and 10% smaller than the diameter of the pillars of the master mold in the 700 nm and 1 µm interspace arrays respectively. The interspace of the pits of the PDMS mold was 2% smaller than that of the pillars of the master mold in both arrays.

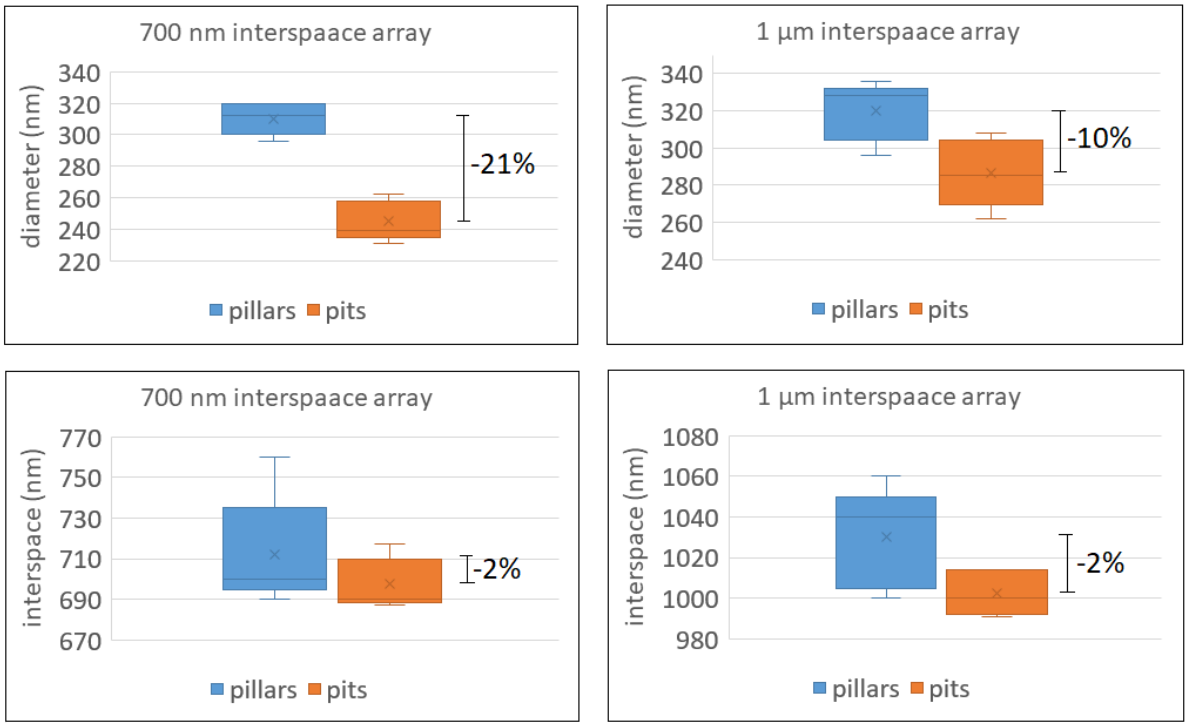

Figure 3.3. Comparison between the diameter and the interspace of the pillars on the master mold and the resultant pits on the hybrid PDMS mold.

3.2. Pattern transfer into the final substrate using TNL

3.2.1. Planar fused silica substrate

3.2.1.1. Thermal nanoimprinting process

Before thermal nanoimprinting, the hybrid PDMS mold was placed on top of the substrate with the patterns facing towards the substrate. Then the sample (the substrate with the hybrid PDMS mold) was placed between two plates and the imprinting force was applied on it (Figure 2.4 d, Figure 3.4).

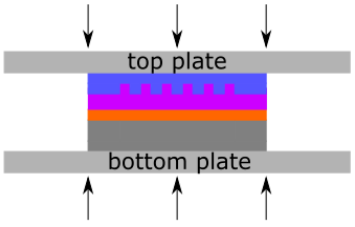

Figure 3.4. Schematic illustration of the imprinting setup for the planar fused silica substrate.

Tilted view SEM images of the pillars formed on PMMA at 250 N and at two different imprinting temperatures (140 °C and 180 °C) are shown in Figure 3.5. The dimensions of the pillars were measured using Gwyddion software and the effect of the imprinting temperature on pillar height and aspect ratio (AR) is shown in Figure 3.6. At 140 °C, the pits of the PDMS mold were imprinted as pillars into the PMMA with an AR of 0.32 in the case of 700 nm interspace array and 0.41 in the case of 1 µm interspace array (Figure 3.6). At 180 °C, the AR of the pillars increased to 1.29 for both arrays (Figure 3.6).

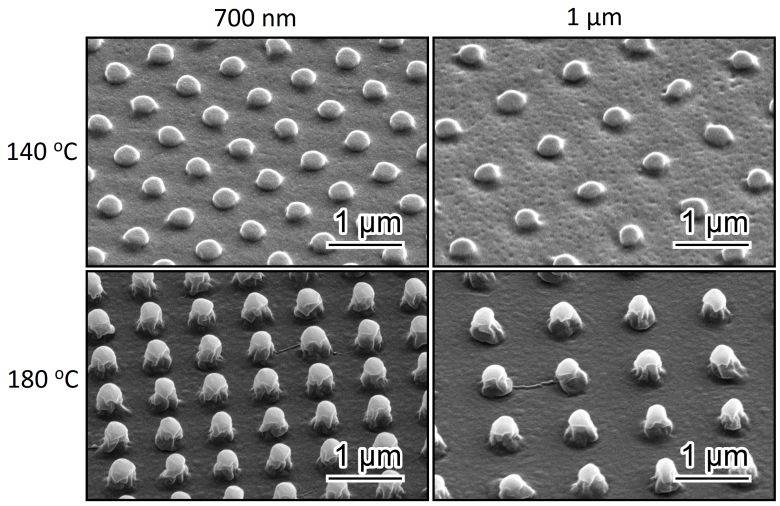

Figure 3.5. 45° tilted view SEM images of the PMMA pillars imprinted on planar fused silica substrates at 250 N.

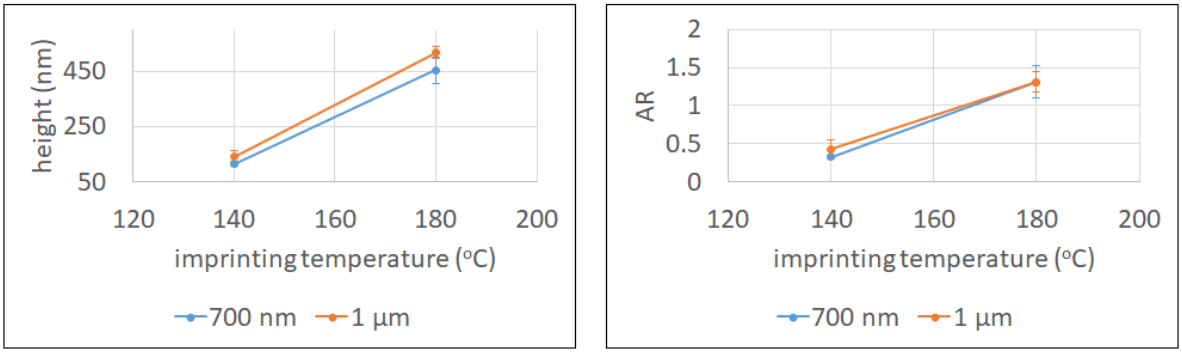

Figure 3.6. Effect of the imprinting temperature on pillar height and AR of the PMMA pillars imprinted on planar fused silica substrates at 250 N.

3.2.1.2. Etching the residual PMMA layer

The morphology of the PMMA pillars - after removing the residues of PMMA rest in between the pillars - was imaged using SEM (Figure 3.7). After following this step, one can have access to the surface of the Cr layer, with PMMA as a mask on top of it.

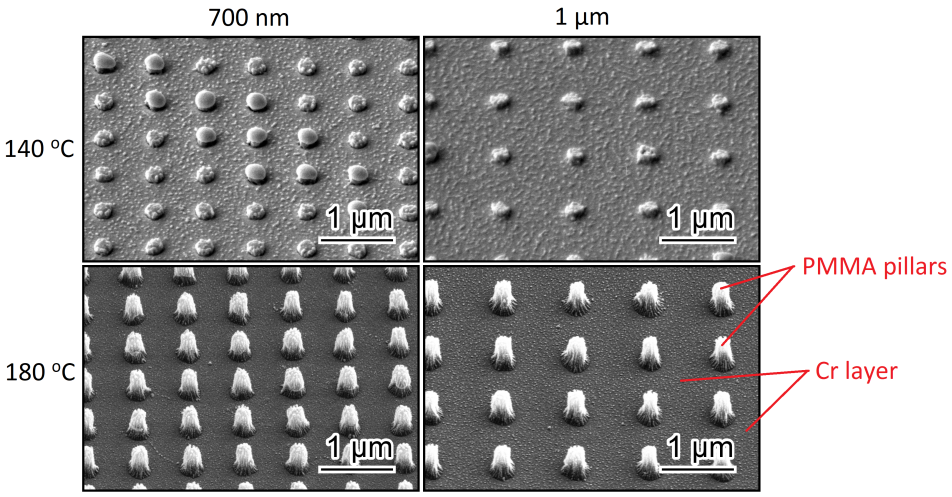

Figure 3.7. 45° tilted view SEM images of the PMMA pillars on the Cr layer on planar fused silica substrates.

3.2.1.3. Etching the Cr layer

To have access to the surface of the fused silica substrate, the Cr layer (thickness = 30 nm) was etched using PMMA as the mask. The remaining patterns consisted of Cr at the bottom that was protected by PMMA and was not etched, and the PMMA mask that was already there (Figure 3.8). This way, the Cr spots that remained made up a mask on the planar fused silica substrate.

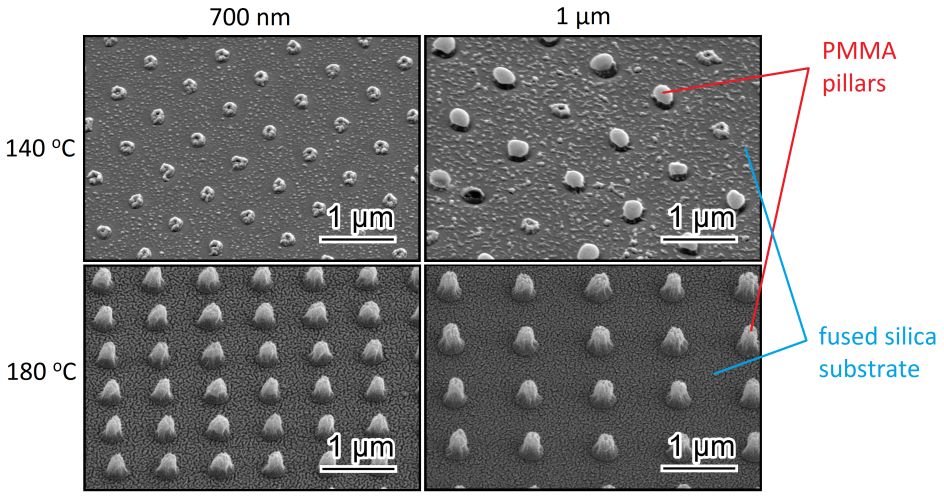

Figure 3.8. 45° tilted view SEM images of the PMMA/Cr mask on planar fused silica substrates.

3.2.1.4. Transferring patterns into the planar fused silica substrate

After chemically removing the PMMA, the planar fused silica substrate was etched with Cr as the mask. ICP RIE of the fused silica substrate through the Cr mask produced pillars into the bulk of the substrate. The pillars had a cylindrical shape (Figure 3.9). The dimensions of the resultant pillars were measured using Gwyddion software and the values of average and standard deviation were calculated (Table 3.1). A comparison between the size of the

resultant pillars on the planar fused silica substrates and the pillars on the master mold is shown in Figure 3.10. The pillars of the two substrates were 9% and 11% shorter in the 700 nm interspace arrays, and 16% and 6% shorter in the 1 µm interspace arrays compared to the pillars of the master mold. The diameter of the pillars of the substrate imprinted at 140 °C was smaller in both arrays (19% and 23%) than the diameter of the pillars of the master mold. The diameter of the pillars of the substrate imprinted at 180 °C was almost the same as the diameter of the pillars of the master mold in the 700 nm interspace array and about 16% higher in the 1 µm interspace array. Finally, the difference in the interspace was equal to or less than 3% for both substrates in both arrays.

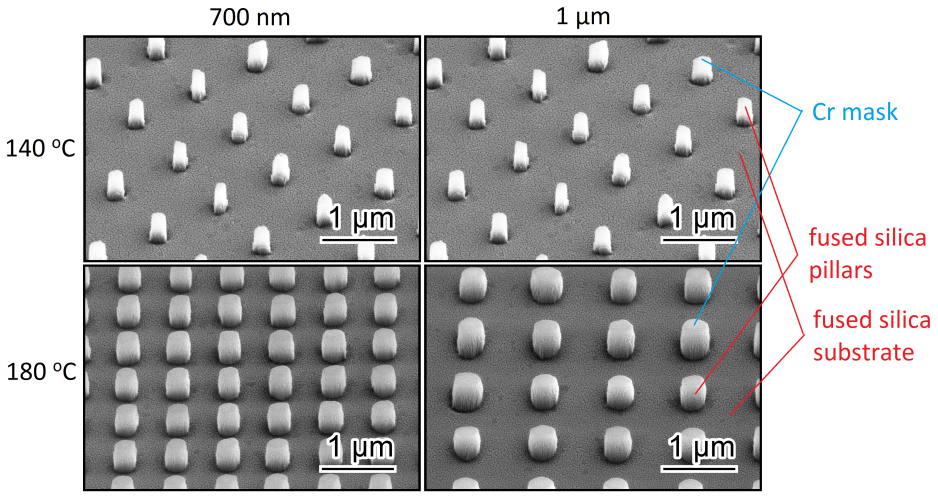

Figure 3.9. 45° tilted view SEM images of the pillars on planar fused silica substrates.

		700 nm	1 µm
interspace (nm)	140 °C	736 ± 15	1048 ± 8
	180 °C	743 ± 15	1043 ± 23
height (nm)	140 °C	606 ± 44	588 ± 23
	180 °C	593 ± 35	654 ± 48
diameter (nm)	140 °C	249 ± 19	243 ± 14
	180 °C	312 ± 26	370 ± 10
AR	140 °C	2.43 ± 0.16	2.42 ± 0.20
	180 °C	1.91 ± 0.20	1.76 ± 0.12

Table 3.1. Dimensions of the pillars fabricated into planar fused silica substrates.

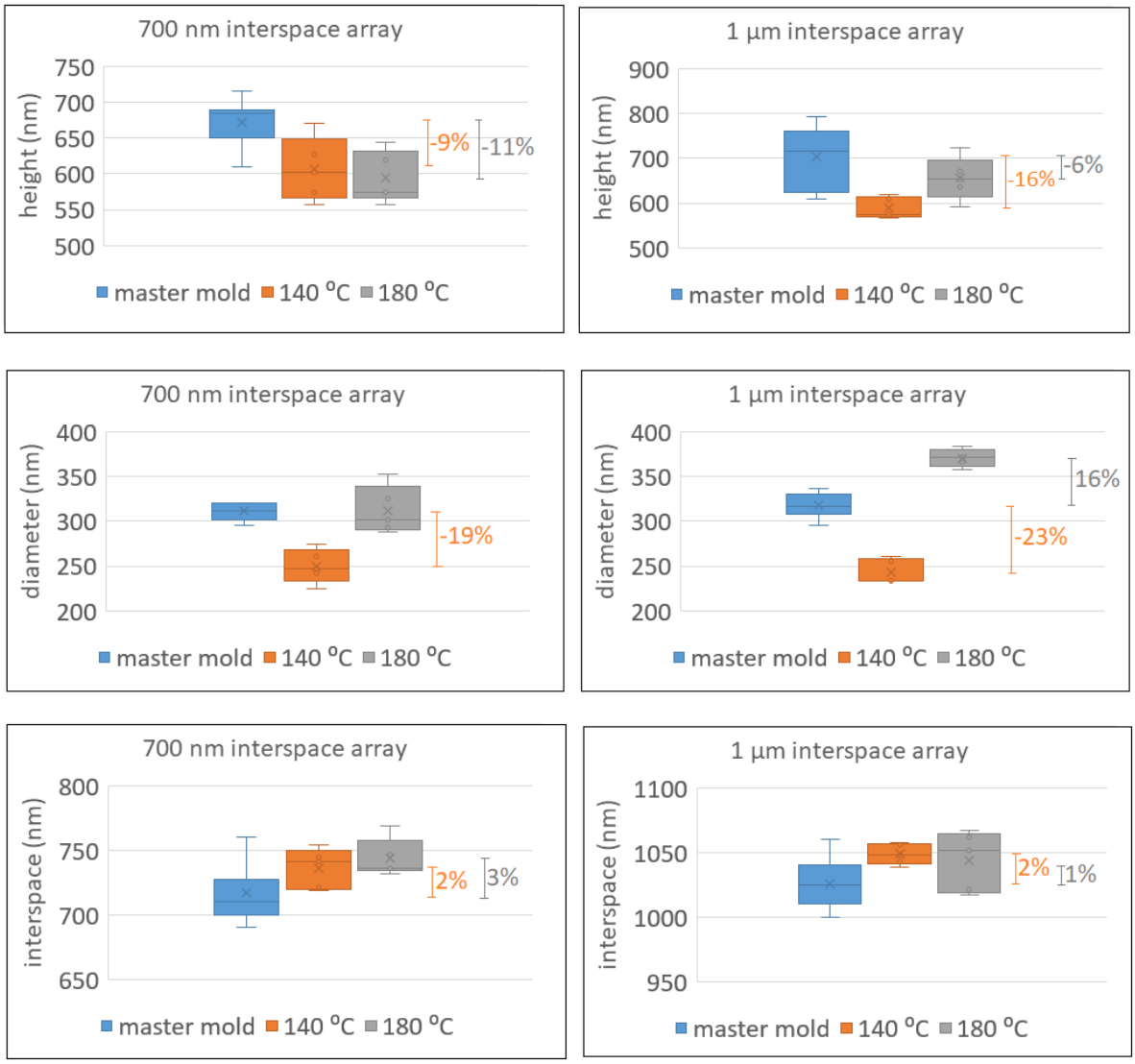

Figure 3.10. Comparison between the height, the diameter, and the interspace of the pillars on the master mold, the pillars on the planar fused silica substrate imprinted at 140 °C, and the pillars on the planar fused silica substrate imprinted at 180 °C.

3.2.2. Curved substrate (BK7 lens)

3.2.2.1. Thermal nanoimprinting process

Before thermal nanoimprinting, the hybrid PDMS mold was placed on top of the curved substrate with the patterns facing towards the substrate. On top of the PDMS mold, a support structure made of PDMS was placed (Figure 3.11). Thereafter, the sample (the substrate with the hybrid PDMS mold and the support structure) was placed between two plates that applied the imprinting force in a "sandwich" like manner on it (Figure 3.11). Four other peripheral support structures made of PDMS were also placed along with the sample in the imprinting system (Figure 3.11). A convex and a concave lens after thermal imprinting are shown in Figure 3.12.

Thermal imprinting on convex lenses was initially conducted at 140 °C and for two force values (1250 N and 2500 N) (Figure 3.13). In both cases, the result was PMMA pillars with

AR less than 1 (Figure 3.14). The higher force (2500 N) resulted in higher pillars. More specifically, the pillar height increased from 132 nm to 210 nm in the 700 nm interspace array and from 150 nm to 190 nm in the 1 µm interspace array (Figure 3.14).

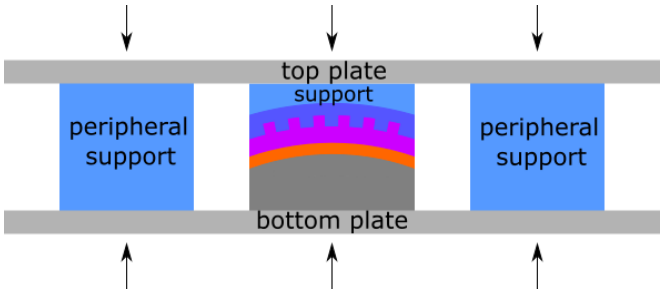

Figure 3.11. Schematic illustration of the imprinting setup for curved substrates.

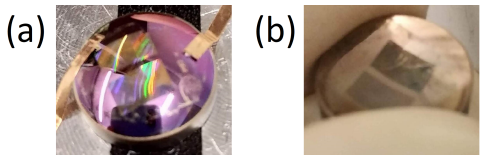

Figure 3.12. a) Convex and b) concave lenses containing two arrays of imprinted pillars.

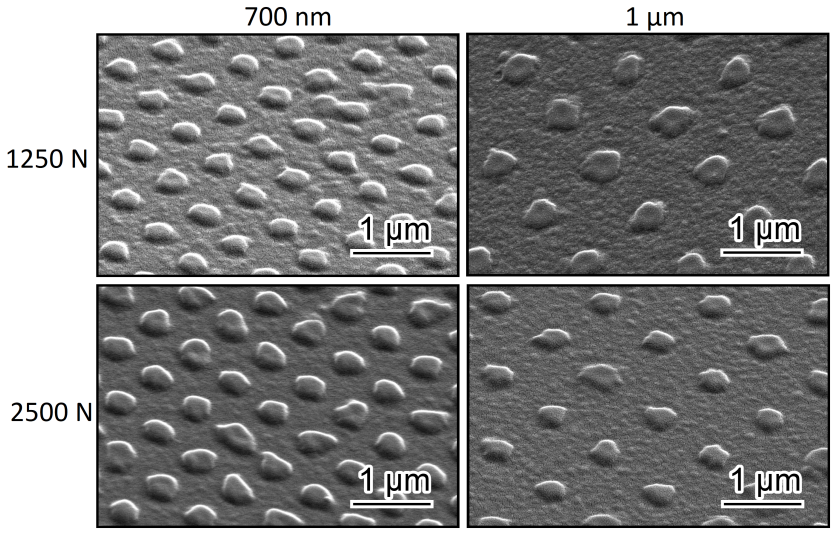

Figure 3.13. 45° tilted view SEM images of the PMMA pillars imprinted on convex substrates at 140 °C.

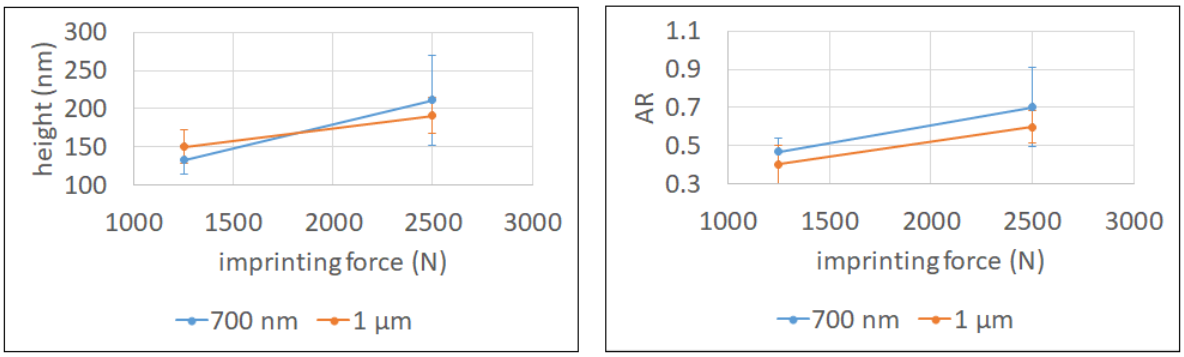

Figure 3.14. Effect of the imprinting force on pillar height and AR of the PMMA pillars imprinted on convex substrates at 140 °C.

Next, thermal imprinting on convex lenses was conducted at 1250 N at three different imprinting temperatures (140 °C, 160 °C, and 180 °C) (Figure 3.15). The dimensions of the pillars were measured and the effect of the imprinting temperature on pillar height and AR is shown in Figure 3.16. Indicatively, pillar height increased from 132 nm at 140 °C to 370 nm at 160 °C and finally, to 721 nm at 180 °C in the 700 nm interspace array (Figure 3.16).

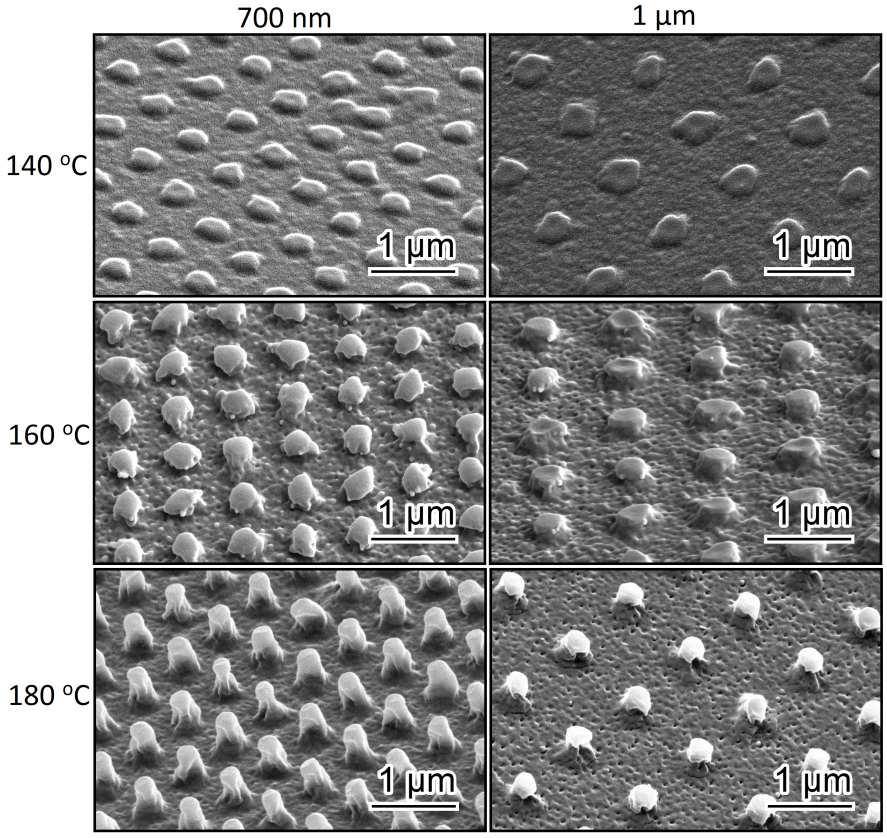

Figure 3.15. 45° tilted view SEM images of the PMMA pillars imprinted on convex substrates at 1250 N.

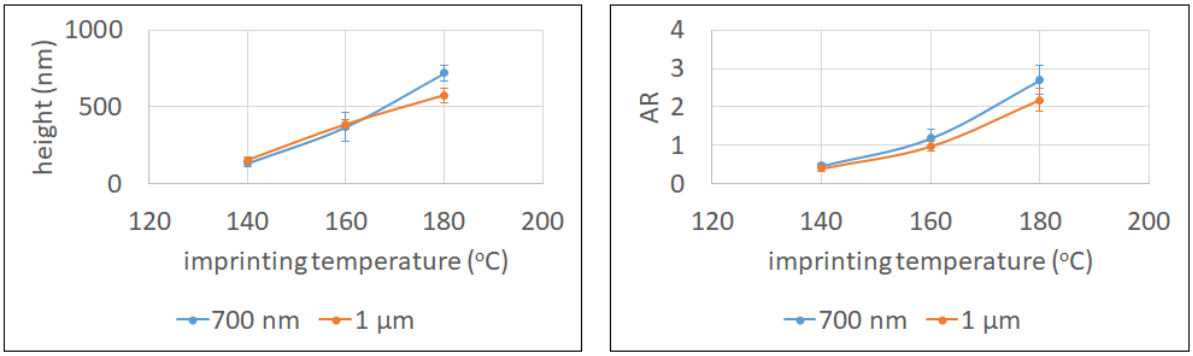

Figure 3.16. Effect of the imprinting temperature on pillar height and AR of the PMMA pillars imprinted on convex substrates at 1250 N.

3.2.2.2. Etching the residual PMMA layer

The morphology of the pillars formed at 1250 N and 180 °C - after removing PMMA rest in between the pillars - was imaged using SEM (Figure 3.17). After following this step, one can have access to the surface of the Cr layer, with PMMA as a mask on top of it.

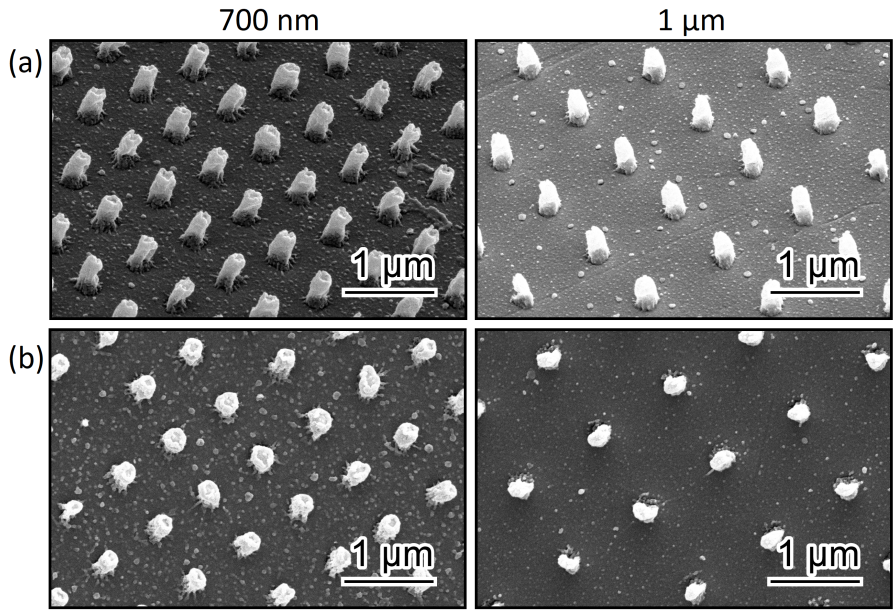

Figure 3.17. a) 45° tilted view and b) top view SEM images of the PMMA pillars on the Cr layer on the convex substrate imprinted at 1250 N and 180 °C.

3.2.2.3. Etching the Cr layer

To have access to the surface of the curved substrate, the Cr layer was etched using PMMA as a mask. The remaining patterns consisted of Cr at the bottom that was protected by PMMA and was not etched, and the PMMA mask that was already there (Figure 3.18). This way, the Cr spots that remained made up a mask on the curved substrate.

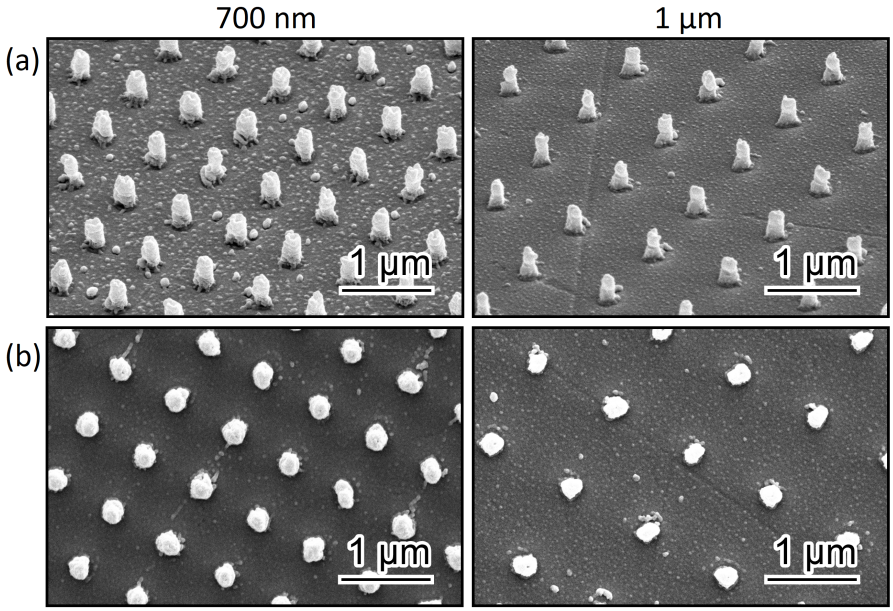

Figure 3.18. a) 45^{o} tilted view and b) top view SEM images of the PMMA/Cr mask on the convex substrate imprinted at 1250 N and 180 °C.

3.2.2.4. Transferring patterns into the curved substrate

After chemically removing the PMMA, ICP RIE was performed on the BK7 substrate. The process did not etch the substrate and a thin film was formed on the lens and detached from its surface (delamination) (Figure 3.19, Figure 3.20).

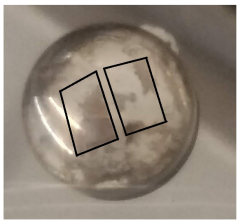

Figure 3.19. Image of the lens after ICP RIE. In the image, the arrays are outlined.

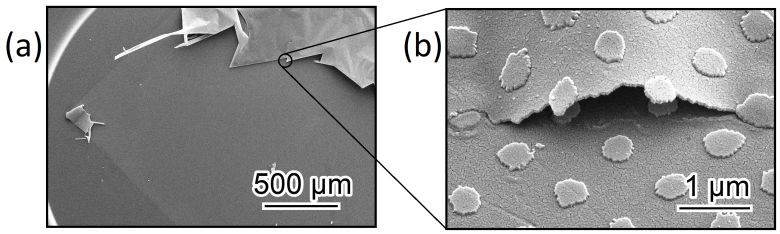

Figure 3.20. SEM images of the BK7 lens after ICP RIE. a) Top view of the thin film and b) 45^{o} tilted view of the pillars.

Thereafter, the substrate was further etched for 4 mins and 10 mins (Figure 3.21). No change was observed in the morphology that was already obtained from the initial etching. The interspace and diameter of the resultant pillars of the 700 nm interspace array

increased by 10% and 11% compared to the corresponding values of the pillars of the master mold. The interspace and diameter of the resultant pillars of the 1 µm interspace array increased by 5% and 57% respectively. The height of the pillars for both arrays was 87% smaller that than the height of the pillars on the master mold.

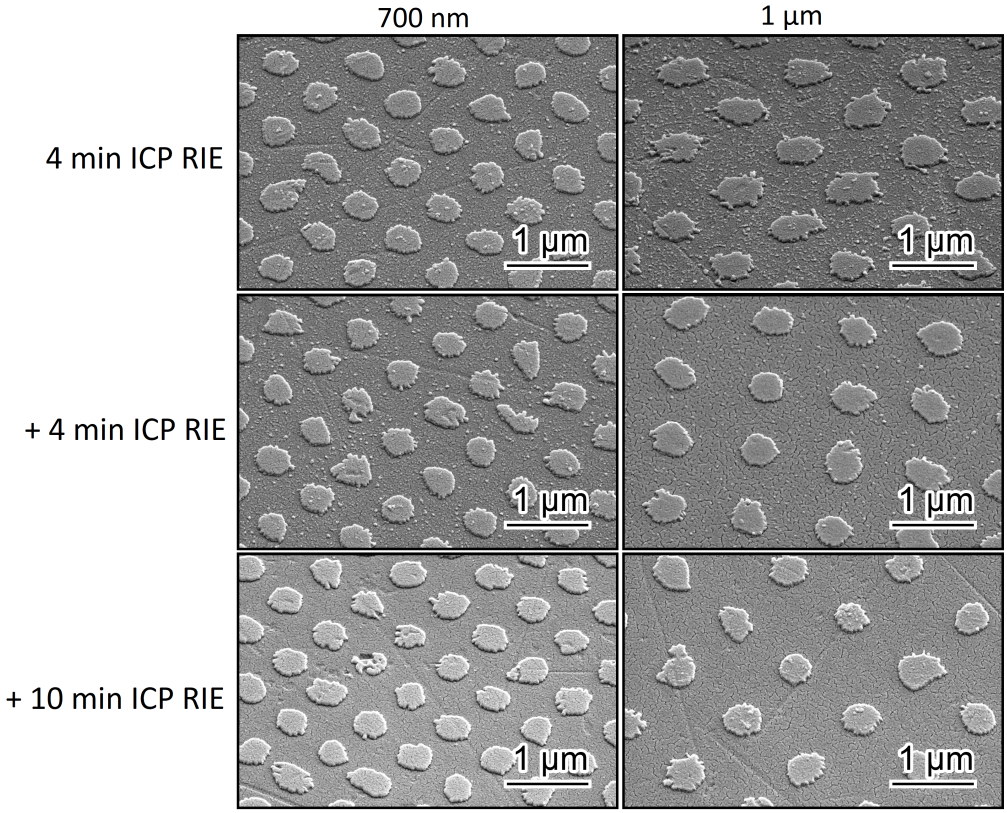

Figure 3.21. 45^{o} tilted view SEM images of the BK7 pillars after several ICP RIE steps on the convex substrate.

We hypothesized that the problem is caused by the metal impurities (*i.e.*, BO, BaO, KO, Na2O [24]) in BK7 material that stop etching. With an aim to expose a pure material to etching species, a relatively thick layer of SiO_2 (2 µm) was deposited on the lens substrate and then, the process steps described in Figure 2.9 were followed. However, after 4 min ICP RIE, the etching did not happen and the pillars were not transferred into the SiO_2 layer (Figure 3.22).

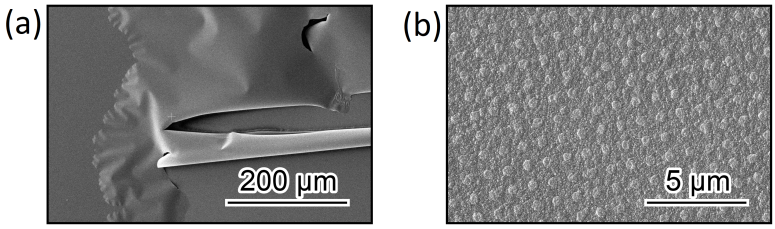

Figure 3.22. Top view SEM images of SiO_2 deposited lens after 4 min etching. a) Delamination phenomenon and b) short pillars on the substrate.

4

Discussion

4.1. Hybrid PDMS mold

The sequential application of hPDMS and PDMS during the molding process guaranteed the reliable replication of the patterns of the master mold into the PDMS mold. PDMS is a soft and elastic material (bulk modulus 2 N/mm^2 [25]). As a result, patterns smaller than 500 nm made of PDMS tend to deform and/or collapse [25]. Therefore, a harder material is needed for high-resolution replication of the pillars, and hPDMS is commonly used for this purpose [26–28]. It has been experimentally confirmed that hPDMS maintains the structural integrity and the shape of patterns with feature sizes down to 10 nm [29]. This way, a highly flexible and durable hybrid PDMS mold containing high-resolution pits is obtained, that can be used several times (without being damaged) as the mold for the following imprinting process.

The diameter of the resultant pits on the PDMS mold was consistently smaller than the diameter of the pillars of the master mold (Figure 3.3). A hypothesis to explain this difference could be that the lower interspacing does not allow the PDMS to fully sink into the pillars. Since pillars are not perfect cylinders, the base diameter is bigger than the top diameter and this results in pits with a much smaller diameter in the denser pillar array (700 nm interspace array). On the other hand, the difference in interspace was quite smaller. Therefore, the interspacing of the arrays was not influenced by the replica molding process. This size reduction is the result of PDMS shrinkage during the thermal curing process and is quite typical in replica molding using PDMS [30]. Also, the reduction of the interspace observed in these experiments (about 2%) (Figure 3.3) is close to the value reported by Madsen *et. al.* [30] (1.07%) who quantified PDMS shrinkage in different conditions (temperature, curing time, PDMS base to curing agent ratio) including the conditions used in our experiments (*i.e.*, 40 ^{o}C, 16 hrs, 10:1) and by measuring a feature very similar to our interspace.

Replica molding is a high-throughput high-resolution experimentally convenient patterning technique. After the first replica molding, a second replica molding could have been done on the resultant mold for the direct fabrication of curved substrates containing pillars. The only limitation of this technique is that it only enables us to replicate patterns into polymers. To be able to transfer the patterns into the substrate of interest, other techniques such as TNL can be employed.

4.2. Pattern transfer into the final desired substrate

4.2.1. Planar fused silica substrate

4.2.1.1. Thermal nanoimprinting process

TNL on planar substrates was performed at two imprinting temperatures and resulted in an increase of the AR of the imprinted PMMA pillars at the higher temperature (Figure 3.6). This result showed the effect of temperature on TNL. The mechanism behind this lies in the effect temperatures above T_g have on the mobility of the molecular chains of the polymer [31]. Below T_g, carbon chains are frozen in place and the material behaves like a rigid solid [31]. At T_g (105 °C for PMMA [32]), carbon chains start to move and the material transits from a rigid state to a rubbery state [31]. As the temperature further increases (140 °C and 180 °C in these experiments), more chains start to move making the polymer softer, and thus, greater deformations can be induced under the same loading conditions.

4.2.1.2. Etching the residual PMMA layer

RIE of PMMA successfully created a PMMA mask on the underlying Cr layer (Figure 3.7). Although PMMA pillars with two different heights were formed at two different imprinting temperatures, for both cases, 2 min O_2 plasma RIE was enough to etch the residues of PMMA rest in between the pillars. As expected, the mask that resulted from the sample imprinted at the higher temperature was thicker.

4.2.1.3. Etching the Cr layer

In both samples (the one imprinted at 140 °C and the one imprinted at 180 °C), the PMMA pillars with different heights were used as the mask to etch the 30 nm thick Cr layer (Figure 3.8). The remaining PMMA pillars in both samples indicate that the mask with the small thickness (the one imprinted at 140 °C) was adequately thick to be used as a mask for Cr etching. After this process, PMMA was removed from both samples leaving a 30 nm thick Cr mask on the substrate material.

4.2.1.4. Transferring patterns into the fused silica substrate

The obtained substrates containing pillars (the one imprinted at 140 °C and the one imprinted at 180 °C) were compared to the master mold in order to evaluate how similar they were (Figure 3.10). The pillars of the two substrates were smaller in height than the pillars of the master mold (Figure 3.10). This means that the etching time should be increased in order to obtain higher pillars. On the other hand, the diameter of the pillars of the substrate imprinted at 140 °C was smaller in both arrays than the diameter of the pillars of the master mold (Figure 3.10). The diameter of the pillars imprinted at 180 °C was almost the same as the diameter of the pillars of the master mold in the 700 nm interspace array and higher in the 1 μm interspace array (Figure 3.10). While the height of the pillars depends on the thickness of the Cr mask and the etching time, the diameter of the pillars depends on the diameter of the Cr mask spots. The Cr mask spots are the result of the previous two steps (TNL and PMMA RIE) and since the PMMA RIE step was also the same for both samples, the conclusion is that the temperature during TNL can be used to control the diameter of

the pillars. Finally, the interspace was slightly influenced (Figure 3.10). Although some imperfections change the morphology of the resultant structures during the middle steps, at the end by optimization of the involved process steps, the dimensions of the final patterns on the fused silica substrates were fairly close to the values of the master mold.

4.2.2. Curved substrate

4.2.2.1. Thermal nanoimprinting process

Traditional imprinting systems have planar surfaces for imprinting on planar substrates. Thermal imprinting on curved substrates requires suitable setups that can bring the mold in conformable contact with the curved substrate. For this purpose, Chen *et. al.* [33] used a setup that consisted of two chambers with the flexible mold separating them as a diaphragm. The substrate was placed below the mold and during the imprinting, the pressure in the two chambers was controlled so that the flexible mold was inflated and brought in conformable contact with the substrate [33]. This system allowed them to imprint with a uniform force distribution on the substrate and also, allows imprinting on substrates of arbitrary curvatures [33]. A simpler approach by Choi *et. al.* [18], included no setup. They simply placed the mold on top of the substrate and applied gentle force with the fingers in order to remove air bubbles and achieve conformable contact with the substrate [18].

The system used in this project was a traditional imprinting system for imprinting on planar substrates. Two setup modifications were applied on it. The first setup modification was the addition of an elastic PDMS structure on top of the hybrid PDMS mold through which the imprinting force was applied indirectly to the mold (Figure 2.8). This was done for two reasons. The first reason was because the imprinting plates were planar and the substrate surface was curved. Executing the experiment without this modification would end up in the force being applied only at the top of the lens. This could probably result in damaging the hybrid PDMS mold, the lens, and machine parts. The second reason was because an elastic and soft intermediate structure was necessary in order to distribute the imprinting force on the whole surface of the lens which would not happen with a rigid structure. With the PDMS support structure in place, the imprinting force was distributed more uniformly on the whole lens' surface area. The second setup modification was the addition of peripheral elastic PDMS support structures (Figure 2.8). The reason was that the surface area of the sample was much smaller than the surface area of the imprinting plates. Therefore, there was a high chance of the imprinting force not being uniformly applied on the substrate's surface area, especially if the sample was not placed exactly in the middle of the plate. Also, even if the force was distributed uniformly, applying the whole force in such a small surface area would cause damage to machine parts. Moreover, the addition of the four peripheral supports in the imprinting setup resulted in a five times bigger imprinting surface area compared to the planar substrate experiments. Thus, in order to keep the force applied on the sample the same as in the planar substrate experiments, imprinting force was also increased five times (1250 N) from the imprinting force value of the planar substrate experiments (250 N).

Imprinting at two different forces resulted in a slight increase in height of the pillars and an AR still smaller than 1 (Figure 3.14). Therefore, it was decided to continue the experiments at 1250 N so that the mechanical stress applied to the hybrid PDMS mold was kept to a minimum. As expected from the planar substrate experiments, the height of the

patterns was greatly increased with the increasing imprinting temperature (Figure 3.16). Therefore, by controlling the imprinting temperature, one could fabricate PMMA pillars with different heights on the curved substrate. Finally, the thermal imprinting protocol was established at 1250 N and 180 °C. It must be highlighted that the planar substrate experiments confirmed that the pillar height achieved at the minimum temperature (140 °C), even small is adequate to be used as a mask and generate pillars on the final substrate.

4.2.2.2. Transferring patterns into the curved substrate

Although RIE of PMMA and Cr on the curved substrate showed the same results as in the planar substrate experiments, etching of the substrate material (BK7 glass) was problematic. The process resulted in small AR pillars even after several etching attempts and every time a thin film (delamination) was generated on the lens and detached from it (Figure 3.20). BK7 glass in contrast to fused silica - on which the etching protocol was originally developed - contains impurities that were first assumed to be the cause of the delamination. In an attempt to fix this problem, a thick layer of SiO_2 was deposited on the lens before the process so that the layer to etch during the final ICP RIE step would be SiO_2 and not BK7 glass. Since the ICP RIE protocol was successful on fused silica which has a high content of SiO_2, it was assumed that it should also work on pure SiO_2. However, still the etching ended up with small AR pillars and delamination (Figure 3.22).

This confirmed that there might be another reason that causes delamination and/or inhibits etching. The lenses are much thicker than the planar fused silica substrates (4.5 mm compared to 0.5 mm) that are traditionally used in such processes. This could result in heat built-up in the large volume of the lens and somehow induce delamination. The relatively high thickness of the non-conductive lens stops heat transfer during the etching process.

5

Conclusion

This report presented a novel facile work that was conducted to develop a process for the fabrication of sub-micron pillars on flat and curved substrates made of glass. To do so, fused silica specimen containing two arrays of sub-micron pillars, one with a center-to-center interspacing of 700 nm and one with a center-to-center interspacing of 1 µm, each on an area of 3x5 mm^2 was used as the master mold. Then, to overcome the challenges of fabrication techniques, including time and cost, soft lithography using hybrid PDMS was used to replicate the pillars as the pits into the hybrid PDMS. The dimensions and morphology of the replicated patterns were assessed using SEM. As PDMS is not the material of choice for many applications, we used TNL as a facile, inexpensive, and high-throughput technique to transfer the patterns on the hybrid PDMS into desired flat/curved substrates. The process parameters were adjusted to have the most precise dimensions transferred. The height of the final patterns can be tuned by optimizing the applied force, imprinting temperature, the thickness of the thermoplastic resist and mask, and etching parameters.

6

Outlook

Although in this research, we could nicely and accurately transfer the patterns on the master mold into the final substrate of interest (fused silica here), transferring them into the curved substrate (BK7 lens here) was more challenging. However, we could transfer our desired patterns into the PMMA layer coated on the lens substrate. Here we present some other strategies that may help to transfer patterns into the substrate underneath:

1. Ion beam etching could be used instead of RIE in order to transfer the pillars directly into the substrate using the PMMA template formed after imprinting. During ion beam etching, energetic ions collide with atoms on the etched substrate transferring energy and momentum to the lattice of the substrate [34]. When the energy transferred to an atom during bombardment exceeds the chemical binding energy, the atom is ejected from the lattice [34]. Ion beam etching has a resolution of tens of nm which is adequate for the much bigger size of our pillars and can etch any material [35].

2. Another solution regarding the approach where the lens was coated with SiO_2 would be to perform the last etching step in small time intervals with cooling steps in between. If the hypothesis of heat build-up during ICP RIE is correct, then by executing etching at small consecutive time steps with cooling steps in between, the temperature of the substrate can be kept under a specified threshold, and delamination may not occur. Since the etching protocol was developed on fused silica and the result was satisfying, the chances to be able to etch successfully SiO_2 are high. So, the objective is to avoid delamination that occurs during this process.

The aim of this project was to develop a process for the fabrication of patterns on curved substrates made of hard materials. The reason was that (as mentioned in the Introduction) studies have shown that pillars and surface curvature separately can modulate the behavior of cells related to bone healing and thus, the next step is to investigate the combined effect of those cues. Also, since Ti is the dominant material choice for bone implants, creating pillars on curved substrates made of Ti is the obvious choice. Fused silica and BK7 were the starting point and the hard material substitutes for these experiments. Therefore, the next step would be to modify this process so that it can transfer patterns into Ti.

Finally, the process is highly adjustable in terms of materials and etching techniques. The fact that it did not work in this modulation does not mean it cannot be completed and further developed. The important part is the establishment of TNL as a suitable method to fabricate highly ordered, high-resolution pillars with control over their size on curved

substrates. Based on this first step, this process can be completed and/or other processes can emerge.

A

Replica molding/Hybrid PDMS fabrication protocol

A.1. Hydrophobic treatment

1. Place the master mold in the center of a small petri dish (∅30) with the pillars facing upwards.

2. Expose the master mold to 100 µl OCTYLTRICHLOROSILANE (Sigma Aldrich, U.S.A.) vapor for 1hr in a desiccator to make its surface hydrophobic.

A.2. hPDMS molding protocol

1. In a small petri dish, add 0.85 g ((7.0-8.0% VINYLMETHYLSILOXANE) – DIMETHYLSILOXANE COPOLYMER, TRIMETHYLSILOXY TERMINATED, 800-1,200 cSt) (Gelest, U.S.A.).

2. Add 3 µl (PLATINUM-DIVINYLTETRAMETHYLDISILOXANE COMPLEX; 2% Pt in xylene) (Gelest, U.S.A.).

3. Add 2 µl (2,4,6,8-Tetramethyl-2,4,6,8-tetravinylcyclotetrasiloxane) (Sigma Aldrich, U.S.A.).

4. Mix for 5 min.

5. Leave petri dish in a desiccator for 30 min.

6. Add 0.25 g ((25-35% METHYLHYDROSILOXANE) – DIMETHYLSILOXANE COPOLYMER, TRIMETHYLSILOXANE TERMINATED, 25-35 cSt).

7. Mix for 3 min.

8. Leave petri dish in a desiccator for a short amount of time, no more than 10 min.

9. Pour 2 drops on the master mold and spin coat for 40 sec at 1000rpm.

10. Leave petri dish containing the master mold in the oven for 20 min at 60 °C.

A.3. PDMS molding protocol

1. In a petri dish, add small amount of PDMS base (Sigma Aldrich, U.S.A.) and PDMS curing agent (Sigma Aldrich, U.S.A.) in a ratio 10:1. The total amount must be at least 0.5 g.

2. Mix for 5 min.

3. Once the 20 min incubation of the hPDMS protocol is done, add 0.5 g of PDMS on the master mold in the petri dish.

4. Leave petri dish cotaning the master mold in a desiccator for 20 min.

5. Leave the petri dish containing the master mold in the oven for 16 hrs at 40 °C.

6. Once the temperature treatment is finished, cut off the patterned part and peel it off very gently from the master mold.

B

Supports fabrication

B.1. PDMS molding protocol

1. Place a lens in the center of a petri dish (or another container).
2. In a petri dish, add PDMS base (Sigma Aldrich, U.S.A.) and PDMS curing agent (Sigma Aldrich, U.S.A.) in a ratio 10:1. The total amount must be enough to fill the container with the lens in it.
3. Mix for 5 min.
4. Pour PDMS in the container with the lens in it. Pour enough PDMS so that it covers the lens for at least 3 mm above it.
5. Leave the container in a desiccator until there are no air bubbles left in the PDMS mixture.
6. Leave the container in the oven for 16 hrs at 40 °C.
7. Once the temperature treatment is finished, demold the lens and cut off the PDMS structure in appropriate pieces.

References

[1] R. A. Potyrailo, H. Ghiradella, A. Vertiatchikh, K. Dovidenko, J. R. Cournoyer, and E. Olson, "Morpho butterfly wing scales demonstrate highly selective vapour response," *Nature Photonics*, vol. 1, no. 2, pp. 123–128, 2007.

[2] T. Badloe, I. Kim, and J. Rho, "Moth-eye shaped on-demand broadband and switchable perfect absorbers based on vanadium dioxide," *Scientific Reports*, vol. 10, no. 1, pp. 1–8, 2020.

[3] K. Nakata, M. Sakai, T. Ochiai, T. Murakami, K. Takagi, and A. Fujishima, "Antireflection and self-cleaning properties of a moth-eye-like surface coated with tio2 particles," *Langmuir*, vol. 27, no. 7, pp. 3275–3278, 2011.

[4] Y. T. Cheng, D. Rodak, C. Wong, and C. Hayden, "Effects of micro-and nano-structures on the self-cleaning behaviour of lotus leaves," *Nanotechnology*, vol. 17, no. 5, p. 1359, 2006.

[5] M. Zhang, S. Feng, L. Wang, and Y. Zheng, "Lotus effect in wetting and self-cleaning," *Biotribology*, vol. 5, pp. 31–43, 2016.

[6] W.-X. Su, C.-Y. Wu, and Y.-C. Lee, "Anti-reflection nano-structures fabricated on curved surface of glass lens based on metal contact printing lithography," *Microelectronic Engineering*, vol. 214, pp. 15–20, 2019.

[7] T. Kamibayashi, H. Kuwae, A. Nobori, S. Shoji, and J. Mizuno, "Fabrication of self-standing curved film with pillar arrays by large area spherical soft-uv imprint lithography," in *2017 International Conference on Electronics Packaging (ICEP)*, pp. 148–151, IEEE, 2017.

[8] D. S. Widyaratih, P.-L. Hagedoorn, L. G. Otten, M. Ganjian, N. Tümer, I. Apachitei, C. W. Hagen, L. E. Fratila-Apachitei, and A. A. Zadpoor, "Towards osteogenic and bactericidal nanopatterns?," *Nanotechnology*, vol. 30, no. 20, p. 20LT01, 2019.

[9] M. Ganjian, K. Modaresifar, M. R. Ligeon, L. B. Kunkels, N. Tümer, L. Angeloni, C. W. Hagen, L. G. Otten, P.-L. Hagedoorn, I. Apachitei, *et al.*, "Nature helps: toward bioinspired bactericidal nanopatterns," *Advanced Materials Interfaces*, vol. 6, no. 16, p. 1900640, 2019.

[10] E. K. Yim, R. M. Reano, S. W. Pang, A. F. Yee, C. S. Chen, and K. W. Leong, "Nanopattern-induced changes in morphology and motility of smooth muscle cells," *Biomaterials*, vol. 26, no. 26, pp. 5405–5413, 2005.

[11] T. Sjöström, L. E. McNamara, R. D. Meek, M. J. Dalby, and B. Su, "2d and 3d nanopatterning of titanium for enhancing osteoinduction of stem cells at implant surfaces," *Advanced healthcare materials*, vol. 2, no. 9, pp. 1285–1293, 2013.

[12] S. Park, D. Kim, S. Park, S. Kim, D. Lee, W. Kim, and J. Kim, "Nanopatterned scaffolds for neural tissue engineering and regenerative medicine," in *Cutting-Edge Enabling Technologies for Regenerative Medicine*, pp. 421–443, Springer, 2018.

[13] H. J. Jang, Y. J. Kim, Y. J. Yoo, G. J. Lee, M. S. Kim, K. S. Chang, and Y. M. Song, "Double-sided anti-reflection nanostructures on optical convex lenses for imaging applications," *Coatings*, vol. 9, no. 6, p. 404, 2019.

[14] K. Haest, "Development of a photovoltaic ceramic roof tile," 2014.

[15] I. Park, S. H. Ko, H. Pan, C. P. Grigoropoulos, A. P. Pisano, J. M. Fréchet, E.-S. Lee, and J.-H. Jeong, "Nanoscale patterning and electronics on flexible substrate by direct nanoimprinting of metallic nanoparticles," *Advanced Materials*, vol. 20, no. 3, pp. 489–496, 2008.

[16] Z. Li, Y. Gu, L. Wang, H. Ge, W. Wu, Q. Xia, C. Yuan, Y. Chen, B. Cui, and R. S. Williams, "Hybrid nanoimprint- soft lithography with sub-15 nm resolution," *Nano letters*, vol. 9, no. 6, pp. 2306–2310, 2009.

[17] J. Chen, C. Gu, H. Lin, and S.-C. Chen, "Soft mold-based hot embossing process for precision imprinting of optical components on non-planar surfaces," *Optics express*, vol. 23, no. 16, pp. 20977–20985, 2015.

[18] W. M. Choi and O. O. Park, "The fabrication of submicron patterns on curved substrates using a polydimethylsiloxane film mould," *Nanotechnology*, vol. 15, no. 12, p. 1767, 2004.

[19] V. Bhingardive, L. Menahem, and M. Schvartzman, "Soft thermal nanoimprint lithography using a nanocomposite mold," *Nano Research*, vol. 11, no. 5, pp. 2705–2714, 2018.

[20] S. J. Callens, R. J. Uyttendaele, L. E. Fratila-Apachitei, and A. A. Zadpoor, "Substrate curvature as a cue to guide spatiotemporal cell and tissue organization," *Biomaterials*, vol. 232, p. 119739, 2020.

[21] M. Ganjian, L. Angeloni, M. J. Mirzaali, K. Modaresifar, C. W. Hagen, M. K. Ghatkesar, P.-L. Hagedoorn, L. E. Fratila-Apachitei, and A. A. Zadpoor, "Quantitative mechanics of 3d printed nanopillars interacting with bacterial cells," *Nanoscale*, vol. 12, no. 43, pp. 21988–22001, 2020.

[22] K. Nojiri, *Dry etching technology for semiconductors*. Springer, 2015.

[23] "Eksma Optics." `https://eksmaoptics.com/`. Accessed: 2021-06-27.

[24] P. W. Leech, "Reactive ion etching of quartz and silica-based glasses in cf4/chf3 plasmas," *Vacuum*, vol. 55, no. 3-4, pp. 191–196, 1999.

[25] T. W. Odom, J. C. Love, D. B. Wolfe, K. E. Paul, and G. M. Whitesides, "Improved pattern transfer in soft lithography using composite stamps," *Langmuir*, vol. 18, no. 13, pp. 5314–5320, 2002.

[26] J. J. Heikkinen, E. Peltola, N. Wester, J. Koskinen, T. Laurila, S. Franssila, and V. Jokinen, "Fabrication of micro-and nanopillars from pyrolytic carbon and tetrahedral amorphous carbon," *Micromachines*, vol. 10, no. 8, p. 510, 2019.

[27] A. Angelin, U. Bog, R. Kumar, C. M. Niemeyer, and M. Hirtz, "Writing behavior of phospholipids in polymer pen lithography (ppl) for bioactive micropatterns," *Polymers*, vol. 11, no. 5, p. 891, 2019.

[28] Q. Yu, S. Braswell, B. Christin, J. Xu, P. M. Wallace, H. Gong, and D. Kaminsky, "Surface-enhanced raman scattering on gold quasi-3d nanostructure and 2d nanohole arrays," *Nanotechnology*, vol. 21, no. 35, p. 355301, 2010.

[29] A. Pandey, S. Tzadka, D. Yehuda, and M. Schvartzman, "Soft thermal nanoimprint with a 10 nm feature size," *Soft Matter*, vol. 15, no. 13, pp. 2897–2904, 2019.

[30] M. H. Madsen, N. A. Feidenhans, P.-E. Hansen, J. Garnæs, and K. Dirscherl, "Accounting for pdms shrinkage when replicating structures," *Journal of Micromechanics and Microengineering*, vol. 24, no. 12, p. 127002, 2014.

[31] A. Shrivastava, "1 - introduction to plastics engineering," in *Introduction to Plastics Engineering* (A. Shrivastava, ed.), Plastics Design Library, pp. 1–16, William Andrew Publishing, 2018.

[32] A. Jacobo-Martín, M. Rueda, J. J. Hernández, I. Navarro-Baena, M. A. Monclús, J. M. Molina-Aldareguia, and I. Rodríguez, "Bioinspired antireflective flexible films with optimized mechanical resistance fabricated by roll to roll thermal nanoimprint," *Scientific reports*, vol. 11, no. 1, pp. 1–15, 2021.

[33] J. Chen, C. Gu, H. Lin, and S.-C. Chen, "Soft mold-based hot embossing process for precision imprinting of optical components on non-planar surfaces," *Opt. Express*, vol. 23, pp. 20977–20985, Aug 2015.

[34] P. G. Glöersen, "Ion- beam etching," *Journal of Vacuum Science and Technology*, vol. 12, no. 1, pp. 28–35, 1975.

[35] R. E. Lee, "Microfabrication by ion-beam etching," *Journal of Vacuum Science and Technology*, vol. 16, no. 2, pp. 164–170, 1979.